



Short communication

Iron modified titanium–hafnium binary oxides as catalysts in total oxidation of ethyl acetate



Tanya Tsoncheva^{a,*}, Radostina Ivanova^a, Jiří Henych^b, Nikolay Velinov^c, Martin Kormunda^d, Momtchil Dimitrov^a, Daniela Paneva^c, Michaela Slušná^{b,e}, Ivan Mitov^c, Vaclav Štengl^b

^a Institute of Organic Chemistry with Centre of Phytochemistry, BAS, Bulgaria

^b Materials Chemistry Department, Institute of Inorganic Chemistry AS CR v.v.i., 25068 Řež, Czech Republic

^c Institute of Catalysis, BAS, Sofia, Bulgaria

^d Faculty of Sciences, University of Jan Evangelista Purkyně, Ceske Mladeze 8, 400 96 Usti nad Labem, Czech Republic

^e Faculty of Environment, University of Jan Evangelista Purkyně, Kralova Vysina 7, 400 96 Usti nad Labem, Czech Republic

ARTICLE INFO

Article history:

Received 6 January 2016

Received in revised form 10 March 2016

Accepted 24 March 2016

Available online 17 April 2016

Keywords:

Titania–hafnia binary oxides

Iron modifications

Support effect

Ethyl acetate oxydation

ABSTRACT

Multicomponent iron–titanium–hafnium oxide materials with different compositions were prepared by combination of homogeneous precipitation with urea and incipient wetness impregnation techniques and tested as catalysts for ethyl acetate oxidation as representative VOCs. Nitrogen physisorption, XRD, Raman, UV–Vis, XPS, Mössbauer spectroscopy and TPR analyses reveal co-existence of substituted $\text{Fe}_x\text{Ti}_{1-x}\text{O}_2$ oxide, finely dispersed iron oxide species with superparamagnetic behavior and well crystallized $\alpha\text{-Fe}_2\text{O}_3$ particles, which relative part depends on hafnium content in titania lattice. The effect of phase composition on the catalytic behavior of these materials in ethyl acetate oxidation was discussed.

© 2016 Elsevier B.V. All rights reserved.

1. Introduction

The knowledge of the specific effects within the multi-component nanostructured metal oxides is prerequisite for the optimization of their properties. Recently, titanium oxide has received much attention due to its superior optical, electrical, mechanical and catalytic properties combined with non-toxicity and cost effectiveness [1]. The introduction of dopant into TiO_2 lattice may significantly affect the electronic band edges or introduce impurity states in the band gap [2]. Formation of $\text{Fe}_x\text{Ti}_{1-x}\text{O}_2$ [3,4], mixture of $\text{Fe}_x\text{Ti}_{1-x}\text{O}_2$ and superparamagnetic hematite particles [5] or mixture of $\text{Fe}_x\text{Ti}_{1-x}\text{O}_2$ and pseudo brookite Fe_2TiO_5 phases [6] were registered after TiO_2 doping with iron. Segregation of $\alpha\text{-Fe}_2\text{O}_3$ phase was reported with the increasing of iron content up to 10% in [7], while Bonamali et al. [8] did not observed its formation even at 50 wt% Fe. However, to the best of our knowledge, there are only few reports on hafnium-doped TiO_2 . Using density functional theory, Lezhong et al. [9] reported that Hf incorporation in TiO_2 leads to narrower band gap, but no experimental evidence has been still reported. No data for the multi-component Ti–Hf–Fe oxide system are still available.

The aim of current investigation is to demonstrate the possibility to control the state of supported on titania–hafnia binary oxides iron species by simple variation of the support composition. Pioneer investigations on the catalytic behavior of these materials in total oxidation of ethyl acetate as representative VOCs are carried out.

2. Experimental

2.1. Materials

Hafnium-doped titania samples were prepared by homogeneous hydrolysis of aqueous solution of TiOSO_4 and HfOSO_4 with urea as a precipitation agent according to the procedure described in [10–12]. Typically, 100 g of TiOSO_4 were dissolved in 1 L hot water acidified with 10 ml 98% H_2SO_4 . After dilution in 4 L distilled water, HfOSO_4 was added for the preparation of binary materials. The pH of the initial solution of TiOSO_4 and HfOSO_4 was 2–4. Then, the solution was mixed with 400 g urea and the mixture was heated at 373 K for 6 h. During the heating, the urea started to decompose and the pH of the solution increased gradually. At the end of the precipitation procedure the pH of the solution became neutral or slightly alkaline pH (7–8). Iron modifications (12 wt%Fe) were obtained by incipient wetness impregnation of thus obtained composites using 0.2 M aqueous solution of $\text{Fe}(\text{NO}_3)_3 \cdot 9\text{H}_2\text{O}$. The impregnated samples were dried at room temperature for 24 h and then, treated in air at 773 K for 2 h for precursor

* Corresponding author at: Institute of Organic Chemistry with Centre of Phytochemistry, BAS, Sofia, Ak.G. Bontchev str.bl.9, Bulgaria
E-mail address: tsoncheva@orgchm.bas.bg (T. Tsoncheva).

Table 1Samples composition, specific surface area (S_{BET}), total pore volume (V_t) and specific activity (SA) for TiO_2 , binary TiO_2 - HfO_2 oxides and their iron modifications.

Sample	Support composition, wt%				Fe, wt%	S_{BET} , $\text{m}^2 \text{g}^{-1}$	V_t , $\text{cm}^3 \text{g}^{-1}$	SA, $\% \text{m}^{-2} \text{g} * 10^2$
	Ti	Hf	O	Hf/Ti + Hf				
TiO_2	60.0	0.0	40.0		0.23		319	15
HfTi(0.8)	59.6	0.5	39.9	0.8	0.22		300	11
HfTi(1.8)	59.2	1.1	39.7	1.8	0.23		326	10
HfTi(9.9)	55.6	6.1	38.3	9.9	0.22		307	13
HfTi(14.9)	53.4	9.3	37.3	14.9	0.24		306	11
HfTi(34.8)	43.5	23.2	33.3	34.8	0.32		488	7
HfTi(41.3)	40.0	28.2	31.8	41.3	0.24		463	7
Fe/ TiO_2	60.0	0.0	40.0		0.15	12	131	45
Fe/HfTi(0.8)	59.6	0.5	39.9	0.8	0.15	12	119	34
Fe/HfTi(1.8)	59.2	1.1	39.7	1.8	0.14	12	115	54
Fe/HfTi(9.9)	55.6	6.1	38.3	9.9	0.15	12	112	48
Fe/HfTi(14.9)	53.4	9.3	37.3	14.9	0.16	12	114	47
Fe/HfTi(34.8)	43.5	23.2	33.3	34.8	0.18	12	118	46
Fe/HfTi(41.3)	40.0	28.2	31.8	41.3	0.17	12	145	37

decomposition. The samples were denoted as HfTi(x) and Fe/HfTi(x) for the parent oxides and their iron modifications, respectively, where x is Hf/Hf + Ti ratio (wt%) and data for their composition are listed in Table 1.

2.2. Characterization and catalytic tests

The surface area of the samples was determined from nitrogen physisorption isotherms using a Coulter SA3100 instrument. Elemental analysis was performed by a MiniPal 4.0 energy-dispersive X-ray fluorescence spectrometer. Powder X-ray diffraction patterns were collected on a Bruker D8 Advance diffractometer with $\text{Cu K}\alpha$ radiation. The UV-Vis spectra were recorded on a Jasco V-650 UV-Vis spectrophotometer. Raman spectra were acquired with a Thermo Fischer Scientific DXR Raman microscope. The X-ray photoelectron spectroscopy analyses were measured in high-vacuum chamber equipped with SPECS Xray XR-50 and SPECS PHOIBOS 100 Hemispheric Analyzer. The Mössbauer spectra were obtained at room and liquid nitrogen temperature with a Wissel electromechanical spectrometer. The TPR/TG (temperature-programmed reduction/thermo-gravimetric) analyses were performed on a Setaram TG92 instrument in a flow of 50 vol% H_2 in Ar ($100 \text{ cm}^3 \text{ min}^{-1}$) and heating rate of 5 K min^{-1} .

The ethyl acetate (EA) oxidation was tested under temperature programmed regime in a flow type apparatus ($1.21 \text{ mol}\%$ EA in air, $\text{WHSV} = 100 \text{ h}^{-1}$) equipped with GC for analyses. The selectivity of the obtained products was calculated as $S_i = Y_i/X * 100$, where Y_i was the yield of (i) product and X was the EA conversion.

3. Results and discussion

3.1. Characterization of TiO_2 - HfO_2 binary oxide supports

XRD pattern of pure titania (not shown) exhibits all reflections typical of anatase phase (JCPDS 21-1272). The observed increase in the lattice parameters after doping with Hf (Table 2) indicates incorporation of Hf^{4+} ions into the titania lattice. The increase of Hf content above 15% provokes the formation of amorphous phase. These structural changes are also confirmed by the observed increase in the BET surface area (Table 1) and with the decrease in the intensity of the main E_g mode at 149 cm^{-1} in the Raman spectra (Fig. 1a) [13]. The strong absorption feature in the UV-Vis spectrum of pure TiO_2 (Fig. S1) at ca. 350 nm is due to d-d electronic transition between Ti^{4+} ion and O^{2-} ligand in anatase. No significant changes in the band gap are observed after titania doping with hafnia and this is in contrast with the theoretic calculations reported in [10]. The broad absorption band in the $900\text{--}400 \text{ cm}^{-1}$ region in FTIR spectrum of titania (Fig. S2) could be assigned to Ti-O-Ti bending vibrations [14]. In accordance with [15] the increased

absorption in the $600\text{--}500 \text{ cm}^{-1}$ range for all Hf doped materials could be carefully assigned to the presence of TiHfO_4 structures. The Ti 2p core level spectra (Fig. 2) represent highly resolved peaks at binding energy of 458.5 eV and split about 5.7 eV which is assigned to Ti-O bonds in TiO_2 [16]. The second component at BE of 456.9 eV represents titanium ions in Ti_2O_3 . Note the almost linear increase in the Ti^{3+} content with the increase of Hf amount which could be due to homogeneous incorporation of Hf in titania with the formation of defects (Table 3, Fig. S3). The Hf 4f spectra for all materials (Fig. S4) represent peaks at BE of 19 and 17 eV, which is assigned to Hf^{4+} ions. For all Hf doped titania samples the calculated Hf/Hf + Ti ratio overcomes the expected nominal one (Table 3) indicating high degree of exposure of Hf ions at the surface. On the base of this observation partial segregation of finely dispersed HfO_2 particles over the titania ones could not be excluded. The O1s core level spectra (Fig. S5) could be assumed as superposition of peaks assigned to oxygen in various states, such as H_2O molecules, surface OH- groups as well as to oxygen anions in Ti-O and Hf-O structures. The observed higher oxygen content than the theoretic one (Table 3) indicates high concentration of hydroxyl groups which are usually related to oxygen vacancies [17].

Table 2XRD data for TiO_2 , various TiO_2 - HfO_2 binary oxides and their iron modifications.

Sample	Phase	D, nm	Strain $e * 10^3$, a.u.	a, Å	c, Å
TiO_2	TiO_2 (anatase)	4.3	6.067	3.793	9.518
HfTi(0.8)	TiO_2 (anatase)	5.0	6.179	3.802	9.522
HfTi(1.8)	TiO_2 (anatase)	4.4	8.299	3.801	9.529
HfTi(9.9)	TiO_2 (anatase)	5.1	7.080	3.804	9.545
HfTi(14.9)	TiO_2 (anatase)	5.6	6.338	3.806	9.556
Fe/ TiO_2	TiO_2 (anatase)	4.4	8.273	3.794	9.509
	$\alpha\text{-Fe}_2\text{O}_3$ (hematite)	4.4	8.273	5.041	13.821
Fe/HfTi(0.8)	TiO_2 (anatase)	5.6	6.629	3.795	9.487
	$\alpha\text{-Fe}_2\text{O}_3$ (hematite)	4.5	9.042	5.016	13.813
Fe/HfTi(1.8)	TiO_2 (anatase)	5.9	6.416	3.795	9.491
	$\alpha\text{-Fe}_2\text{O}_3$ (hematite)	5.4	2.709	5.006	13.854
Fe/HfTi(9.9)	TiO_2 (anatase)	5.5	6.787	3.799	9.508
	$\alpha\text{-Fe}_2\text{O}_3$ (hematite)	5.3	8.140	5.043	13.865
Fe/HfTi(14.9)	TiO_2 (anatase)	6.1	5.932	3.804	9.505
	$\alpha\text{-Fe}_2\text{O}_3$ (hematite)	4.5	9.049	5.032	13.872
Fe/HfTi(34.8)	TiO_2 (anatase)	8.4	4.363	3.801	9.522
	$\alpha\text{-Fe}_2\text{O}_3$ (hematite)	5.8	7.586	5.043	13.872
Fe/HfTi(41.3)	TiO_2 (anatase)	9.1	3.223	3.796	9.532
	$\alpha\text{-Fe}_2\text{O}_3$ (hematite)	21.6	2.848	5.052	13.763

 TiO_2 (anatase) S.G.: $I4_1/amd$ (141) – tetragonal. $\alpha\text{-Fe}_2\text{O}_3$ (hematite) S.G.: R-3cH (167) – trigonal.

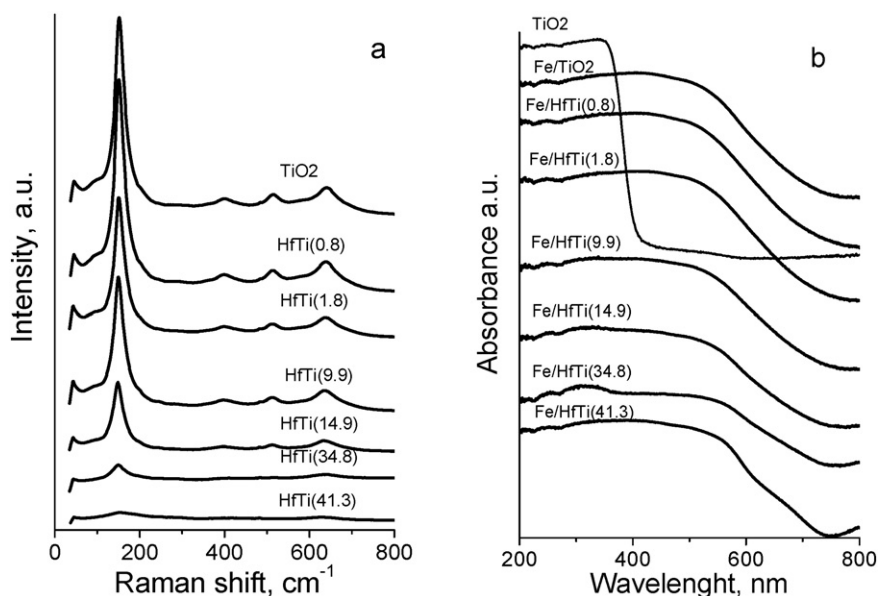


Fig. 1. Raman spectra of TiO_2 and $\text{TiO}_2\text{-HfO}_2$ binary oxides (a) and UV-Vis spectra (b) of their iron modifications.

3.2. Characterization of iron modified $\text{TiO}_2\text{-HfO}_2$ binary oxides

Nitrogen physisorption measurements demonstrate that the high temperature treatment during the modification procedure strongly decreases the specific surface area, which for all iron modifications varies in the $110\text{--}145\text{ m}^2\text{ g}^{-1}$ range (Table 1). XRD patterns indicate presence of anatase phase with particle size of about $5\text{--}9\text{ nm}$ (Table 2). Reflections, typical of hematite phase (JCPDS 33-0664) with average crystallite size of $4\text{--}22\text{ nm}$, are also detected. The observed decrease in the unit cell parameters for all iron modifications could be attributed to the substitution of Ti^{4+} ions by smaller Fe^{3+} ions in anatase lattice. The incorporation of Fe^{3+} ions is also confirmed by the red shift of the absorption band in the UV-Vis spectra (Fig. 1b) [8]. In agreement with XRD data, the increased absorption in the $300\text{--}600\text{ nm}$ region can be

assigned to superposition of bands originated from iron ions in small oligonuclear Fe_xO_y clusters and bulk Fe_2O_3 particles.

Room temperature Mössbauer spectra of all iron modifications are well fitted with sextet and doublet components (Fig. S6). The parameters of sextet component (Table 4) are characteristic for $\alpha\text{-Fe}_2\text{O}_3$ with average crystallite size above 13.5 nm . In accordance with [18] the Db1 component in the spectra with QS of about $1.21\text{--}1.28\text{ mm/s}$ could be assigned to $\text{Fe}_x\text{Ti}_{1-x}\text{O}_2$. The second doublet component with QS of $0.70\text{--}0.78\text{ mm/s}$ can be assigned to smaller $\alpha\text{-Fe}_2\text{O}_3$ particles with superparamagnetic behavior. This assumption is confirmed by the Mössbauer spectra, recorded under the temperature of liquid nitrogen (LNT, Fig. S6, Table 4), where an increase in the relative part of Sx component at the expense of a decrease in the Db2 component is detected. The preservation of a large portion of doublet part in the LNT spectra

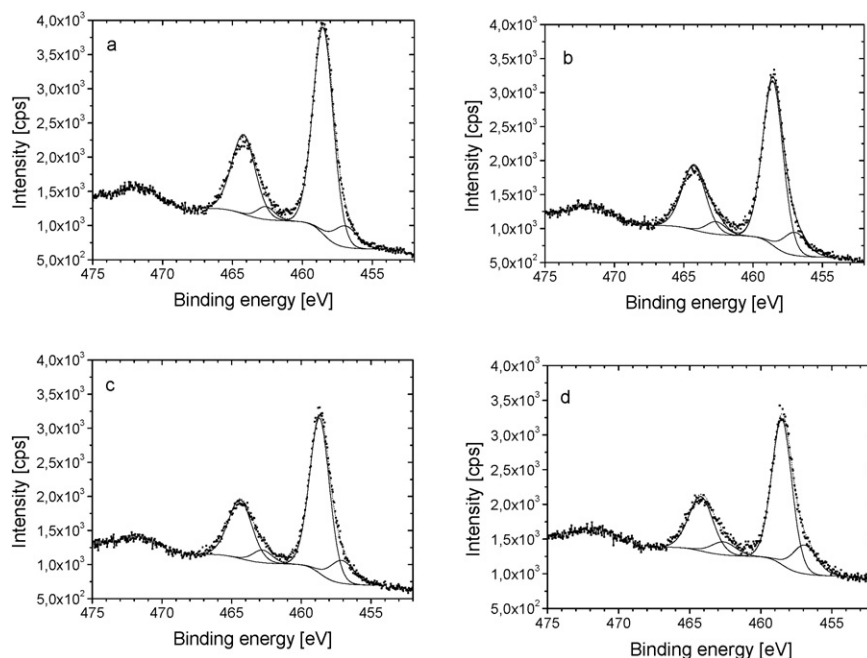


Fig. 2. Ti 2p core level spectra of selected samples: (a) TiO_2 ; (b) $\text{HfTi}(1.8)$; (c) $\text{HfTi}(14.9)$; (d) $\text{HfTi}(34.8)$.

Table 3

Surface composition (at.%) of selected modifications on the base of XPS analyses (in brackets wt%).

Sample	C	Hf	O	Ti	Ti ³⁺ /Ti ³⁺ + Ti ⁴⁺ , %	Hf/Ti + Hf	O/Ti + Hf
TiO ₂	12.38	0	65.01	22.61	11.39		2.87
HfTi(1.8)	10.23	0.28*	65.72	23.77	14.67	1.17(4.4)	2.73
HfTi(14.9)	10.38	1.50	66.39	21.73	15.67	6.45(25.7)	2.85
HfTi(34.8)	20.21	3.73	58.57	17.49	21.88	17.58(44.3)	2.76

Table 4

Mössbauer parametra of iron modifications of TiO₂ and TiO₂-HfO₂ binary oxides.

Sample	Components	IS, mm/s	QS, mm/s	H _{eff} , T	FWHM, mm/s	G, %
Fe/TiO ₂	Sx-α-Fe ₂ O ₃	0.37	-0.24	51.5	0.36	13
	Db1	0.31	1.27	-	0.49	41
	Db2	0.34	0.73	-	0.46	46
Fe/HfTi(0.8)	Sx-α-Fe ₂ O ₃	0.35	-0.18	51.3	0.45	6
	Db1	0.30	1.26	-	0.48	43
	Db2	0.34	0.73	-	0.46	51
Fe/HfTi(1.8)	Sx-α-Fe ₂ O ₃	0.37	-0.24	51.2	0.34	9
	Db1	0.30	1.26	-	0.50	44
	Db2	0.33	0.73	-	0.46	47
Fe/HfTi(9.9)	Sx-α-Fe ₂ O ₃	0.37	-0.24	51.1	0.35	13
	Db1	0.31	1.24	-	0.50	44
	Db2	0.34	0.71	-	0.46	43
Fe/HfTi(9.9) (LNT)	Sx-α-Fe ₂ O ₃	0.45	0.38	53.5	0.40	15
	Db1	0.41	1.24	-	0.48	48
	Db2	0.44	0.72	-	0.41	37
Fe/HfTi(14.9)	Sx-α-Fe ₂ O ₃	0.36	-0.22	51.2	0.37	20
	Db1	0.31	1.21	-	0.49	44
	Db2	0.34	0.70	-	0.42	37
Fe/HfTi(34.8)	Sx-α-Fe ₂ O ₃	0.38	-0.20	51.1	0.38	28
	Db1	0.33	1.28	-	0.45	31
	Db2	0.36	0.76	-	0.43	41
Fe/HfTi(41.3)	Sx-α-Fe ₂ O ₃	0.39	-0.22	51.0	0.37	45
	Db1	0.34	1.26	-	0.50	31
	Db2	0.36	0.78	-	0.41	24

Isomer shift (IS), quadruple splitting (QS), the effective internal magnetic field (H_{eff}), the line widths (FWHM), and the relative weight (G).

reveals existence of hematite-like particles about 4 nm. Thus, we cannot fully exclude partial contribution of the shell of these particles [19] in the Db1 component which renders difficult precise quantitative analyses on the base of relative part of Db1 and Db2. However analyzing the changes in the relative part of Db and Sx components in the spectra with the variations in the support composition (Table 4), one can assume that the incorporation of small amount of Hf⁴⁺ in titania promotes the formation of substituted Fe_xTi_{1-x}O₂ and finely dispersed hematite like particles. We can speculate that these hematite particles form on the interface layer of the substituted Fe_xTi_{1-x}O₂ ones. Moreover, the increase in the degree of occupation of Ti⁴⁺ positions by Hf⁴⁺ in binary oxides results in segregation of larger portion of bulk hematite phase. Taking into account XPS data (Table 3), where a linear dependence between Ti³⁺ and Hf was observed, we assume that Fe³⁺ ions substitute predominantly Ti⁴⁺, but not Ti³⁺ ions into the solid lattice.

The TPR profiles of iron modifications (Fig. 3) represent one significant TPR effect centered at 620–646 K and second, less pronounced one, above 700 K, which according to [20] could be assigned to stepwise reduction of hematite to Fe. The shift of the reduction peaks to lower temperature for all Hf modified materials as compared to pure TiO₂, most pronounced for Fe/HfTi(1.8), indicates presence of finely dispersed Fe₂O₃ particles. The increase in the high temperature TPR effect for the samples with high Hf content confirms the increase in the portion of larger hematite particles. Note that the overall reduction degree for all materials is 42–65% (Table S1). In accordance with Mössbauer data (Table 4), the observed increase in the reduction degree with Hf content increase (Table S1) indicates that these hardly reducible iron ions are mainly included into substituted Fe_xTi_{1-x}O₂ structures.

3.3. Catalytic properties

In Fig. S7 are presented temperature profiles of ethyl acetate oxidation on various Ti–Hf supports and their iron modifications. In order to simplify the comparison between various materials, the temperature dependences only for selected samples are presented in Fig. 4a and the temperature at which 50% conversion (T₅₀) is achieved for all materials are shown in Fig. 4b. Acetaldehyde (AA), ethanol (Et), ethene (C₂) and acetic acid (AcAc) were found as by-products and their distribution

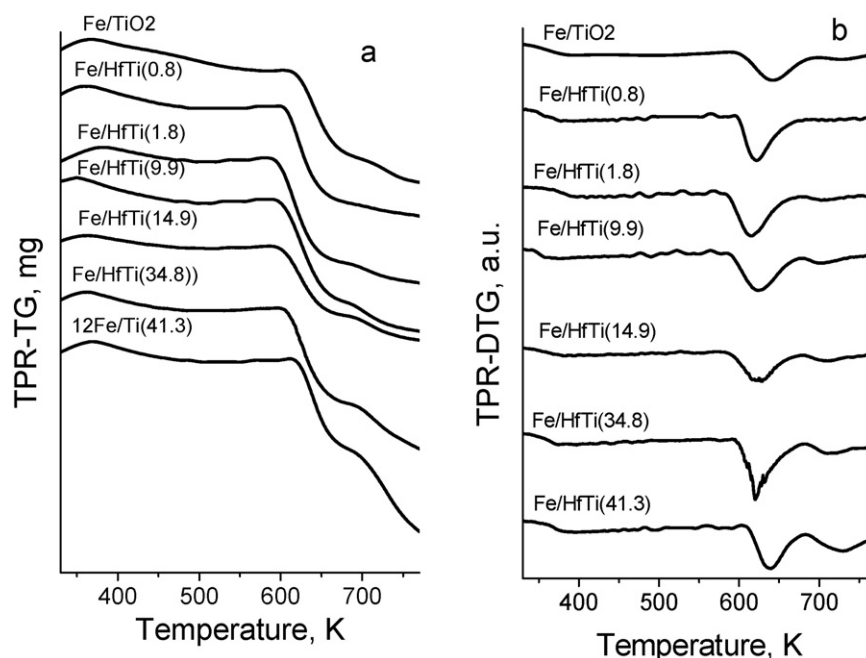


Fig. 3. TPR–TG (a) and TPR–DTG (b) profiles of iron modifications of TiO₂ and TiO₂-HfO₂.

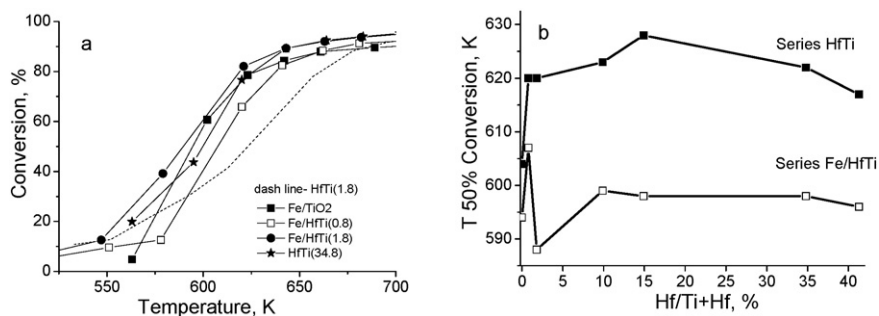


Fig. 4. Temperature dependencies of ethyl acetate conversion for selected catalysts (a) and effect of Hf content on the catalytic activity of various binary oxides and their iron modifications, represented as the temperature at which 50% conversion is achieved (b).

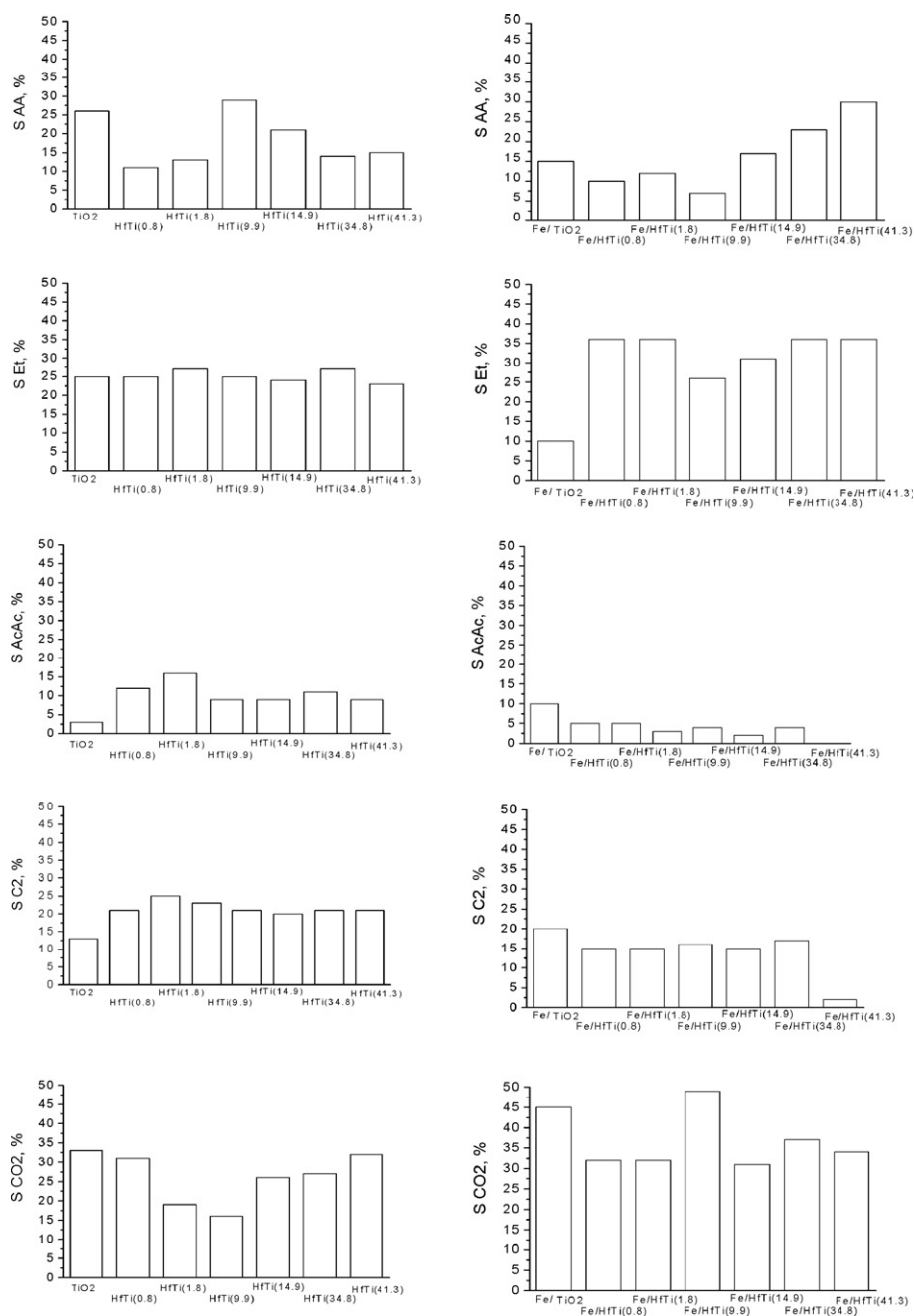


Fig. 5. Selectivity to CO₂ and various by-products (acetaldehyde (AA), ethanol (Et), acetic acid (AcAc) and ethylene (C₂)) for TiO₂ and different TiO₂-HfO₂ oxides (left) and their iron modifications (right) at 45% conversion.

at 45% conversion is compared in Fig. 5. Pure titania and its hafnia modifications represent about 80% conversion above 650 K (Fig. S7). Catalytic activity decrease combined with an increase in the AcAc and C₂ selectivity is observed after titania doping with small amount of Hf (Figs. 4 and 5). The observed slight increase in the catalytic activity of the samples with higher Hf content could be assigned to the increase in the specific surface area of the samples (Tables 1 and 2). In order to precise the discussion and to exclude the role of texture parameters on the catalytic activity, the specific catalytic activity per unit surface area (SA) was calculated (Table 1). For all binary oxides a decrease in SA as compared to pure TiO₂ is observed. However, no clear relation between the changes in SA with Hf increase in the samples is observed. This could be due to lack of homogeneity in the catalytic sites in binary materials. On the base of XPS analyses, we can assume that this could be due to the formation of a mixture of various metal oxide phases, such as TiO₂, HfO₂ and TiO₂-HfO₂, which proportion varies with Hf/Ti ratio. It seems also that the facilitated formation of Ti³⁺ defects after Hf incorporation decreases the number of active Ti⁴⁺-Ti³⁺ redox pairs.

The modification of TiO₂ and TiO₂-HfO₂ composites with iron strongly increases both catalytic activity (Fig. 4, Fig. S7) and CO₂ selectivity (Fig. 5). As compared to the commercial copper catalyst (Fig. S7) and the data reported in the literature (Table S2) these materials represent significantly high catalytic activity. The observed about 4–5-fold increase in the SA after the modification of Ti-Hf oxides with iron clearly indicate its decisive participation in the ethyl acetate oxidation. Note the highest catalytic activity which was registered for Fe/HfTi (1.8), where a big portion of particles with superparamagnetic behavior was observed by Mössbauer analysis (Table 4) and also absence of any simple relation between the iron phase composition and the specific activity of the samples. These features urge the authors to assume different contributions of various iron species in the ethyl acetate oxidation. Taking into account that the ethyl acetate oxidation realizes by Mars van Krevelen mechanism [21], where the release of oxygen from the metal oxide lattice is of primary importance, and also on the base of TPR analysis, we assume the facilitated effect of the formation of finely dispersed hematite particles. The combined Mössbauer and TPR data clearly demonstrate that the increase in the dispersion of hematite particles is promoted by the formation of hardly reducible and probably low active, Fe_xTi_{1-x}O₂ layer. The proportion of various iron species, and the related catalytic properties, could be simply regulated by Hf incorporation in titania lattice. In order to precise the role of various species in this complex multicomponent materials further investigations are in progress.

4. Conclusions

The state of iron species supported on titania-hafnia binary oxides could be easily controlled by support composition. Small amount of Hf in titania facilitates the formation of substituted Fe_xTi_{1-x}O₂ and finely dispersed hematite particles, while the increase of hafnium content promotes segregation of larger hematite particles. The catalytic activity in ethyl acetate oxidation is in a complex relation with sample composition. The best catalytic activity is achieved for iron modification of titania doped with 1.8% Hf, where the presence of relatively large portion of easily reducible hematite particles is observed.

Supplementary data to this article can be found online at <http://dx.doi.org/10.1016/j.catcom.2016.03.014>.

Acknowledgments

Financial support of project DFNI E02/2/2014, and joint research project between ASCR and BAS and Bulgarian-Italian BAS-CNR bilateral

project is acknowledged. This work was also supported by Large Infrastructures for Research, Experimental Development and Innovation – NanoEnvicZ – Nanomaterials and Nanotechnologies for Environmental Protection and Sustainable Future No. LM2015073. The authors thank to Z. Hájková for Raman measurements.

References

- [1] C.T. Fleaca, M. Scarisoreanu, I. Morjan, R. Alexandrescu, F. Dumitrache, C. Luculescu, I.P. Morjan, R. Birjega, A.-M. Niculescu, G. Filoti, V. Kuncser, E. Vasile, V. Danciu, M. Pop, Recent progress in the synthesis of magnetic titania/iron-based, composite nanoparticles manufactured by laser pyrolysis, *Appl. Surf. Sci.* 302 (2014) 198–204.
- [2] Y. Zhang, Y. Shen, F. Gu, M. Wu, Y. Xie, J. Zhang, Influence of Fe ions in characteristics and optical properties of mesoporous titanium oxide thin films, *Appl. Surf. Sci.* 256 (2009) 85–89.
- [3] Y.H. Zhang, A. Reller, Nanocrystalline iron-doped mesoporous titania and its phase transition, *J. Mater. Chem.* 11 (2001) 2537–2541.
- [4] C. Wang, Q. Li, R.D. Wang, Synthesis and characterization of mesoporous iron-doped TiO₂, *J. Mater. Sci.* 39 (2004) 1899–1902.
- [5] R. Janes, L.J. Knightley, C.J. Harding, Structural and spectroscopic studies of iron (III) doped titania powders prepared by sol-gel synthesis and hydrothermal processing, *Dyes Pigments* 62 (2004) 199–212.
- [6] D. Cordischi, N. Burriesci, F. D'Alba, M. Petrerà, G. Polizzotti, M. Schiavello, Structural characterization of Fe/Ti oxide photocatalysts by X-ray, ESR, and Mössbauer methods, *J. Solid State Chem.* 56 (1985) 182–190.
- [7] J.A. Wang, R. Limas-Ballesteros, Quantitative determination of titanium lattice defects and solid-state reaction mechanism in iron-doped TiO₂ photocatalysts, *J. Phys. Chem. B.* 105 (2001) 9692–9698.
- [8] B. Pal, M. Sharon, G. Nogami, Preparation and characterization of TiO₂/Fe₂O₃ binary mixed oxides and its photocatalytic properties, *Mater. Chem. Phys.* 59 (1999) 254–261.
- [9] L. Lezhong, Y. Weiqing, D. Yingchun, Z. Xinghua, First principle study of the electronic structure of hafnium-doped anatase TiO₂, *J. Semicond.* 33 (2012) 012002–012004.
- [10] V. Štengl, S. Bakardjieva, N. Murafa, V. Houšková, K. Lang, Visible-light photocatalytic activity of TiO₂/ZnS nanocomposites prepared by homogeneous hydrolysis, *Micro-porous Mesoporous Mater.* 110 (2008) 370–378.
- [11] O. Daněk, V. Štengl, S. Bakardjieva, N. Murafa, A. Kalendová, F. Opluštil, Nanodispersive mixed oxides for destruction of warfare agents prepared by homogeneous hydrolysis with urea, *J. Phys. Chem. Solids* 68 (2007) 707–711.
- [12] L. Österlund, V. Štengl, A. Mattsson, S. Bakardjieva, P.O. Andersson, F. Opluštil, Effect of sample preparation and humidity on the photodegradation rate of CEES on pure and Zn doped anatase TiO₂ nanoparticles prepared by homogeneous hydrolysis, *Appl. Catal. B Environ.* 88 (2009) 194–203.
- [13] C. Adána, A. Bahamondea, I. Ollerb, S. Malatob, A. Martínez-Ariasa, Influence of iron leaching and oxidizing agent employed on solar photodegradation of phenol over nanostructured iron-doped titania catalysts, *Appl. Catal. B Environ.* 144 (2014) 269–276.
- [14] H. Nur, Modification of titanium surface species of titania by attachment of silica nanoparticles, *Mater. Sci. Eng. B* 133 (2006) 49–54.
- [15] T. Kidchob, P. Falcaro, P. Schiavuta, S. Enzo, P. Innocenzi, Formation of monoclinic hafnium titanate thin films via the sol-gel method, *J. Am. Ceram. Soc.* 91 (2008) 2112–2116.
- [16] Sanjay Mathur, Patrick Kuhn, CVD of titanium oxide coatings: comparative evaluation of thermal and plasma assisted processes, *Surf. Coat. Technol.* 201 (2006) 807–814.
- [17] T. Leshuk, R. Parviz, P. Everett, H. Krishnakumar, R.A. Varin, F. Gu, Photocatalytic activity hydrogenated TiO₂, *ACS Appl. Mater. Interfaces* 5 (2013) 1892–1895.
- [18] Q. Gao, X. Wu, Y. Fan, The effect of iron ions on the anatase/rutile phase transformation of titania (TiO₂) in mica/titania pigments, *Dyes Pigments* 95 (2012) 96–101.
- [19] D. Milivojevic, B. Babic-Stojic, V. Jokanovic, Z. Jaglicic, D. Makovec, N. Jovic, Magnetic properties of ultrasmall iron-oxide nanoparticles, *J. Alloys Compd.* 595 (2014) 153–157.
- [20] S. Bzdón, J. Goralski, W. Maniukiewicz, J. Perkowski, J. Rogowski, M. Szadkowska-Nicze, Radiation-induced synthesis of Fe-doped TiO₂: characterization and catalytic properties, *Radiat. Phys. Chem.* 81 (2012) 322–330.
- [21] S.S.T. Bastos, S.A.C. Carabineiro, J.J.M. Órfão, M.F.R. Pereira, J.J. Delgado, J.L. Figueiredo, Total oxidation of ethyl acetate, ethanol and toluene catalyzed by exotemplated manganese and cerium oxides loaded with gold, *Catal. Today* 180 (2012) 148–154.